Neurotoxicology 70 (2019) 112–121

Contents lists available at ScienceDirect

Neurotoxicology

journal homepage: www.elsevier.com/locate/neuro

Saikosaponin d causes apoptotic death of cultured neocortical neurons by increasing membrane permeability and elevating intracellular Ca^{2+} concentration

Jing Zheng[a,1], Juan Chen[a,1], Xiaohan Zou[a,*], Fang Zhao[a], Mengqi Guo[b], Hongbo Wang[b], Tian Zhang[c], Chunlei Zhang[a], Wei Feng[d], Isaac N. Pessah[d], Zhengyu Cao[a,*]

[a] State Key Laboratory of Natural Medicines and Jiangsu Key Laboratory of TCM Evaluation and Translational Research, School of Traditional Chinese Pharmacy, China Pharmaceutical University, Nanjing, Jiangsu, 211198, China
[b] School of Pharmacy, Key Laboratory of Molecular Pharmacology and Drug Evaluation (Yantai University), Ministry of Education, Yantai University, Yantai, 264005, China
[c] Beijing Key Laboratory of Gene Resource and Molecular Development, College of Life Sciences, Beijing Normal University, Beijing, 100875, China
[d] Department of Molecular Biosciences, School of Veterinary Medicine, University of California, Davis, CA, 95616, USA

ARTICLE INFO

Keywords:
Apoptotic cell death
Ca^{2+} influx
Membrane permeability
Neurotoxicity
Saikosaponins

ABSTRACT

Saikosaponins (SSs) are a class of naturally occurring oleanane-type triterpenoid saponins found in *Radix bupleuri* that has been widely used in traditional Chinese medicine. As the main active principals of *Radix bupleuri*, SSs have been shown to suppress mouse motor activity, impair learning and memory, and decrease hippocampal neurogenesis. In the present study, we investigated the effect of five SSs (SSa, SSb1, SSb2, SSc, and SSd) on neuronal viability and the underlying mechanisms in cultured murine neocortical neurons. We demonstrate that SSa, SSb1 and SSd produce concentration-dependent apoptotic neuronal death and induce robust increase in intracellular Ca^{2+} concentration ($[Ca^{2+}]_i$) at low micromolar concentrations with a rank order of SSd > SSa > SSb1, whereas SSb2 and SSc have no detectable effect on both neuronal survival and $[Ca^{2+}]_i$. Mechanistically, SSd-induced elevation in $[Ca^{2+}]_i$ is the primary result of enhanced extracellular Ca^{2+} influx, which likely triggers Ca^{2+}-induced Ca^{2+} release through ryanodine receptor activation, but not SERCA inhibition. SSd-induced Ca^{2+} entry occurs through a non-selective mechanism since blockers of major neuronal Ca^{2+} entry pathways, including L-type Ca^{2+} channel, NMDA receptor, AMPA receptor, Na^+-Ca^{2+} exchanger, and TRPV1, all failed to attenuate the Ca^{2+} response to SSd. Further studies demonstrate that SSd increases calcein efflux and induces an inward current in neocortical neurons. Together, these data demonstrate that SSd elevates $[Ca^{2+}]_i$ due to its ability to increase membrane permeability, likely by forming pores in the surface of membrane, which leads to massive Ca^{2+} influx and apoptotic neuronal death in neocortical neurons.

1. Introduction

Saikosaponins (SSs) are a class of naturally occurring oleanane-type triterpenoid saponins found in *Radix bupleuri* (Yang et al., 2017), which has been widely used in traditional Chinese medicine for more than two thousand years. The therapeutic properties of SSs have been documented to include relieving fever stemming from infections, hemorrhoids and indigestion, as well as the treatment of liver diseases, such as

Abbreviations: AMPAR, α-amino-3-hydroxy-5-methyl-4-isoxazolepropionic acid receptor; CI, confidence intervals; CNQX, 6-cyano-7-nitroquinoxaline-2,3-dione; CPA, cyclopiazonic acid; DIV, days *in vitro*; DMSO, dimethyl sulfoxide; EGTA, ethylene glycol bis(β-amino-ethylether)tetraacetic acid; ER/SR, endoplasmic/sarcoplasmic reticulum; FDA, fluorescein diacetate; HEPES, 4-(2-Hydroxyethyl)-1-piperazineethanesulfonic acid; IP_3R, inositol trisphosphate receptor; JSR, junctional sarcoplasmic reticulum; KB-R7943, 2-[2-[4-(4-nitrobenzyloxy)phenyl]ethyl]isothiourea; MK-801, dizocilpine maleate; MOPS, 3-morpholinopropanesulfonic acid; MTT, 3-(4,5-dimethylthiazol-2-yl)-2,5-diphenyltetrazolium bromide; NADH, nicotinamide adenine dinucleotide; NMDAR, N-methyl-D-aspartate receptor; PI, propidium iodide; RR, ruthenium red; RyR, ryanodine receptor; SB366791, 4'-Chloro-3-methoxycinnamanilide; SERCA, sarco/endoplasmic reticulum Ca^{2+}-ATPase; SSs, saikosaponins; TG, thapsigargin; TRP, transient receptor potential cation channel; $[^3H]$Ry, $[^3H]$Ryanodine; $[Ca^{2+}]_i$, intracellular Ca^{2+} concentration

* Corresponding authors at: Jiangsu Key Laboratory of TCM Evaluation and Translational Research, School of Traditional Chinese Pharmacy, China Pharmaceutical University, Nanjing, Jiangsu, 211198, China.
E-mail addresses: imzouxiaohan@163.com (X. Zou), zycao1999@hotmail.com (Z. Cao).
[1] Equal Contribution.

https://doi.org/10.1016/j.neuro.2018.11.006
Received 1 September 2018; Received in revised form 1 November 2018; Accepted 14 November 2018
Available online 17 November 2018
0161-813X/

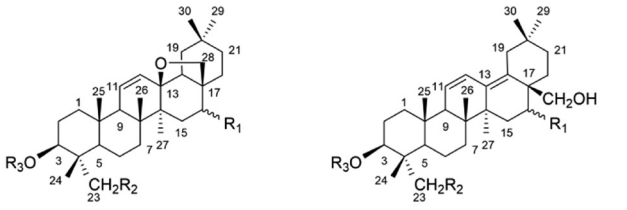

	Type	R_1	R_2	R_3
SSa	I	β-OH	OH	glc (1→3) fuc
SSb1	II	β-OH	OH	glc (1→3) fuc
SSb2	II	α-OH	OH	glc (1→3) fuc
SSc	I	β-OH	H	glc (1→6) [rha (1→4)] glc
SSd	I	α-OH	OH	glc (1→3) fuc

glc = β-D-glucopyranosyl; fuc = β-D-fucopyranosyl; rha = α-L-rhamnopyranosyl

Fig. 1. Chemical structures of five Saikosaponins (SSs). SSs are a class of natural occurring oleanane-type triterpene saponins widely distributed in Radix bupleuri. Type I saikosaponins (SSa, SSc and SSd) possess a cyclic ether bridge linking C13 and C28 while type II (SSb1 and SSb2) are not.

stagnation (qi) and irritability (National Pharmacopoeia Committee NP, 2015). SSs have long been considered the active principals in *Radix bupleuri* products and their potential as therapeutics have been investigated in a variety of disease models. SSs have been reported to display anti-inflammatory (Du et al., 2018; Liu et al., 2014; Lu et al., 2012; Ma et al., 2015; Wang et al., 2018), anti-viral (Fang et al., 2017), anti-tumor (Chen et al., 2016; Li et al., 2017a; Wong et al., 2013; Zhong et al., 2016), and nephroprotective properties (Ma et al., 2015). Their anti-inflammatory activity primarily stems from inhibition of the NF-κB signaling pathway (Du et al., 2018; Fu et al., 2015; Liu et al., 2014; Ma et al., 2015). Among the SSs, saikosaponin d (SSd; Fig. 1) appears to be the most active compound (Yuan et al., 2017).

Results from additional studies have demonstrated the neuroactive properties of SSs. SSd has been reported to suppress stress-induced depressive-like behaviors and alter hippocampal neurogenesis (Li et al., 2017). One of the SSd analogs, saikosaponin a (SSa) significantly reduced seizure severity, duration and prolonged seizure latency in a pentylenetetrazol-induced epileptic seizure model; an action that could be mediated through inhibition of mTOR signaling (Ye et al., 2016). However, recent findings suggest that SSa also enhances glutamate uptake capacity of astrocytes (Gao et al., 2017). In hippocampal neuronal culture models of acquired epilepsy and status epilepticus, SSa effectively terminated spontaneous recurrent epileptic discharges and continuous high-frequency bursts at concentrations below micromolar through a number of mechanisms including inhibition of N-methyl-D-aspartate receptors (NMDAR) or voltage-gated sodium channels, and enhancement 4-aminopyridine-sensitive outward K^+ current (Xie et al., 2013; Yu et al., 2012). In addition to its antiepileptic activity, SSa also displayed analgesic effects in a rat neuropathic pain model induced by chronic constriction injury of the sciatic nerve through a mechanism involving inhibition of p38 MAPK and NF-κB signaling pathways in the spinal cord (Zhou et al., 2014). Finally, SSa suppresses morphine, cocaine and alcohol self-administration, likely through modulation of $GABA_B$ receptor (Maccioni et al., 2016; Yoon et al., 2012, 2013).

Despite the clinical benefits of SSs in a variety of disease models, clinical use of *Radix bupleuri* products produce several severe adverse effects, including pain, allergy, low blood pressure, dizziness, convulsion as well as limb twitching (Ikegami et al., 2006), untoward effects that have precipitated a black box warning on injectable formulations of *Radix bupleuri* by China Food and Drug Administration on May 29th, 2018 (http://cnda.cfda.gov.cn/WS04/CL2050/228214.html). Results from toxicological studies demonstrate that SSd induces cells death in human LO2 hepatocytes and pluripotent stem cell-derived hepatocytes, possibly through disrupting platelet-derived growth factor-β receptor/p38 and activating Fas death receptor within the concentration range capable of producing therapeutic effects (Chen et al., 2013; Li et al., 2017c; Smutny et al., 2018; Zhang et al., 2016). Most recently, SSd has also been demonstrated to produce neurotoxicity. Systematic administration of SSd suppresses motor activity of mice in the open field test, impairs learning and memory in Morris water maze test, and decreases hippocampal neurogenesis, possibly by interfering with the Akt/Foxg1 pathway (Xu et al., 2018). However, the primary molecular mechanism (s) of acute SSd neurotoxicity remains unclear.

Ca^{2+} dynamic controls neuronal development, activity-dependent neurite outgrowth and synaptogenesis (George et al., 2012; Saneyoshi et al., 2008). Significant increase in the intracellular Ca^{2+} concentration ($[Ca^{2+}]_i$) leads to neuronal death (He et al., 2017; Nayler, 1983; Zieminska et al., 2017). SSd has been demonstrated to increase the $[Ca^{2+}]_i$ level which leads to autophagic cell death in HeLa and MCF-7 cancer cells through activation of Ca^{2+}/calmodulin-dependent pathway (Wong et al., 2013). Computational ligand docking and coupled enzyme assays suggest that sarco/endoplasmic reticulum Ca^{2+} ATPase (SERCA) pump may be a molecular target responsible for elevated $[Ca^{2+}]_i$ leading to cell death in cardiomyocytes and hepatocytes (Wang et al., 2017; Wong et al., 2013). It has also been reported that saponins, a class of compounds containing amphiphilic molecular structure with a lipophilic aglycone and a hydrophilic sugar side chain were able to complex with cholesterol to form non-selective cation/anion channels in both biological and artificial membranes (Sudji et al., 2015; Li et al., 2005) which may also mediate extracellular Ca^{2+} influx.

In the present study, we therefore investigated the neurotoxicity of SSs in primary neocortical neuronal cultures and their underlying mechanisms. We demonstrate that SSd produces concentration-dependent apoptotic neuronal death as well as induces robust increase in $[Ca^{2+}]_i$ within the low micromolar concentration range. We also demonstrate that elevation in $[Ca^{2+}]_i$ primarily results from enhanced extracellular Ca^{2+} influx, which likely triggers Ca^{2+}-induced Ca^{2+} release through ryanodine receptor (RyR) activation, but not SERCA inhibition. Further experiments demonstrate that SSd induces elevation in $[Ca^{2+}]_i$ due to its ability to increase the membrane permeability, possibly through forming pores in the surface membrane that leads to massive Ca^{2+} influx and apoptotic neuronal death in neocortical neurons.

2. Materials and methods

2.1. Materials

Saikosaponins (SSa, SSb1, SSb2, SSc, SSd, purity > 98%) were from Chengdu Purify Technology Development Co., Ltd. (Chengdu, Sichuan, China). Calcein-AM was from Shanghai Aladdin Bio-Tech Co., Ltd. (Shanghai, China). Trypsin, DNase I, soybean trypsin inhibitor, neurobasal medium, fetal bovine serum, glutamax, and leupeptin were obtained from Life Technology (Grand Island, NY, USA). Fluorescein diacetate (FDA), propidium iodide (PI), 3-(4,5-dimethylthiazol-2-yl)-2,5-diphenyltetrazolium bromide (MTT), and Hoechst 33342 were from Beyotime Bio-Tech Institute (Shanghai, China). Nifedipine, cyclopiazonic acid (CPA), dizocilpine maleate (MK-801) and 2-[2-[4-(4-nitrobenzyloxy)phenyl]ethyl]isothiourea mesylate (KB-R7943) were purchased from Tocris Bioscience (Ellisville, MO, USA). Poly-L-lysine was from Peptide Institute, Inc. (Osaka, Japan). Fluo-4/AM was from ATT Bioquest (Sunnyvale, CA, USA). Ryanodine was from Ascent Scientific, Inc. (Bristol, UK). [^{3}H]Ryanodine was purchased from PerkingElmer (San Jose, CA, USA; specific activity: 56.6 Ci/mmol). Nicotinamide adenine dinucleotide (NADH) was from Roche Molecular Systems (Pleasanton, CA, USA). D-(+)-glucose, Na_2ATP, MgATP, glycine, ruthenium red (RR), 4-(2-hydroxyethyl)-1-piperazineethanesulfonic acid (HEPES), phenol red, ethylene glycol-bis(β-aminoethyl ether)-N,N,N′,N′-tetraacetic acid (EGTA), cytosine β-D-arabinofuranoside, 6-cyano-7-nitroquinoxaline-2,3-dione (CNQX), 4′-

Chloro-3-methoxycinnamanilide (SB366791), thapsigargin (TG), phosphocreatine, creatine phosphokinase, Arsenazo III, Hoechst 33342, n-decane and 3-morpholinopropanesulfonic acid (MOPS) were purchased from Sigma-Aldrich (St. Louis, MO, USA). Lipid mixture was from Avanti Polar Lipids, Inc. (Alabaster, AL, USA).

2.2. Primary cortical neuron culture

All animal experiment protocols were carried out according to the National Institutes of Health guideline for the care and use of Laboratory animals (NIH Publications No. 8023, revised 1978) and approved by the China Pharmaceutical University and UC Davis Institutional Animal Care and Use Committees. Primary cultures of neocortical neurons were obtained from embryonic day 16-17 C57BL/6 mice (both male and female) as described previously (Cao et al., 2014). Briefly, dissected cerebral cortex was minced and digested with trypsin for 25 min at 37 °C. The dissociated neurons were re-suspended in neurobasal medium supplemented with NS21 (Chen et al., 2010), 0.2 mM glutamax and 5% fetal bovine serum. The dissociated cortical cells were plated onto poly-L-lysine pre-coated (0.5 mg/mL) clear-bottom, black-wall, 96-well imaging plates (BD, Franklin Lakes, NJ, USA) or 12-well plate at densities of 1.5×10^5 cells/well and 1.2×10^6 cells/well, respectively. The medium was changed at days *in vitro* (DIV) 5 and 7 by replacing half the volume of culture medium with serum free neurobasal complete medium. The neurons were maintained at 37 °C with 5% CO_2 and 95% humidity. A final concentration of cytosine β-D-arabinofuranoside (10 μM) was added to the culture medium 24–36 h after plating to prevent the astrocytes proliferation.

2.3. MTT assay

Neocortical neurons cultured in 96-well plate at 7–9 DIV were used to measure the cell viability using MTT assay as described previously (Levitz and Diamond, 1985). Briefly, neurons were continuously exposed to different concentrations of SSs or vehicle control (0.1% DMSO) for 24 h in the culture medium. After aspirating the medium, a volume of 100 μL medium containing 0.5 mg/mL MTT was added to each well and incubated for 10 min at 37 °C. After discarding the medium, a volume of 150 μL DMSO was added to each well. The absorbance was measured at 570 nm and 650 nm in a microplate reader (Tecan Group Ltd., Männedorf, Switzerland) to measure the content of formazan generated in each well.

2.4. FDA/PI and Hoechst 33342 staining

FDA/PI double staining and Hoechst 33342 staining were performed as described previously (Cao et al., 2010; He et al., 2017). Briefly, after exposure to different concentrations of SSs or vehicle control (0.1% DMSO) for 24 h in the culture medium, neurons cultured in 96-well plate were washed for three times using Locke's buffer (in mM: HEPES 8.6, KCl 5.6, NaCl 154, D-glucose 5.6, $MgCl_2$ 1.0, $CaCl_2$ 2.3, and glycine 0.1, adjust pH to 7.4 with NaOH). A volume of 100 μL Locke's buffer containing FDA (5 μg/mL) and PI (1 μg/mL) was then added to each well and incubated in room temperature for 10 min to visualize the live and dead cells. To determine the apoptotic cells, a concentration of 5 μg/mL Hoechst 33342 was added to visualize nuclei. Images were taken with a Nikon eclipse fluorescence microscope (Nikon, Tokyo, Japan) by using DAPI, FITC or Texas Red filters. The numbers of live, dead cells, and condensed nuclei were manually counted in each picture. Data were represented as % dead cells or % apoptotic neurons.

2.5. Intracellular Ca^{2+} monitoring

Neocortical neurons at 7–9 DIV were used to investigate the influence of SSs on $[Ca^{2+}]_i$ as described previously (Cao et al., 2015). In brief, after 45 min loading of Fluo-4/AM at 37 °C, neurons were washed four times with fresh Locke's buffer and loaded into a Fluorescent Imaging Plate Reader ($FLIPR^{Tetra}$; Molecular Devices, CA, USA) incubation chamber. Emission fluorescence at wavelength of 515–575 nm was recorded at a sampling rate of 1 Hz with an excitation wavelength of 470–495 nm. After recording the basal fluorescence for about 200–300 s, different concentrations of SSs were added to corresponding wells using a programmable 96-channel robotic pipetting system and the fluorescent signals were recorded for an additional 400 s. Data were presented as F/F_0, where F is the fluorescent signal at different time point whereas F_0 is the basal fluorescence. The area under curve (AUC) obtained from an epoch of 5 min after addition of SSs was used to compare the influences of SSs on $[Ca^{2+}]_i$.

2.6. Preparation of skeletal muscle (RyR1) and cardiac muscle (RyR2) preparations

Microsomal membrane vesicles enriched RyR1 and SERCA1, and ventricle membrane homogenate preparations enriched in RyR2 were prepared from skeletal muscle of New Zealand White rabbit and C57BL/6 mouse heart ventricles, respectively, as described previously (Cherednichenko et al., 2004; Pessah et al., 1986). Each membrane preparation was kept at −80 °C until use. Protein concentrations were determined using BCA assay kit (Life Technology, Grand Island, NY, USA).

2.7. Measurement of microsomal vesicle Ca^{2+} uptake and efflux

The active uptake and passive release of Ca^{2+} ion from junctional sarcoplasmic reticulum (JSR) vesicles was determined by measuring the differential absorbance of metallochromic Ca^{2+} indicator Arsenazo III at 650–700 nm in an Agilent 8453 UV–vis Spectroscopy System (Agilent Technologies, Santa Clara, CA, USA) at 37 °C as recently described (Feng et al., 2017). The assay solution contained 100 μg/mL of rabbit skeletal muscle JSR, 2 mM MgATP, 10 mM phosphocreatine, 20 μg/mL creatine phosphokinase, and Arsenazo III (250 μM) in reaction buffer (in mM: KCl 100, MOPS 20, $Na_4P_2O_7$ 6, pH7.4). Calcium loading of JSR vesicles was accomplished by three sequential additions of 45 nmole $CaCl_2$. After the final bolus of Ca^{2+} was accumulated into the vesicles, vehicle control (0.1% DMSO) or test compounds was added to determine the Ca^{2+} efflux. To quantified the SSd influence on Ca^{2+} efflux, the Ca^{2+} release rate (nmol Ca^{2+}/sec/mg JSR) was calculated from 60 s right after addition of compounds.

2.8. Measurement of SERCA activity

Activity of SERCA from each membrane preparation was measured using a coupled enzyme assay that monitors the rate of oxidation of NADH at 340 nm using an Agilent 8453 UV–vis diode array spectrophotometer (Agilent Technologies, Santa Clara, CA, USA) as described previously (Ta et al., 2006). After the baselines were established in about 1–2 min, 0.3 mM NADH was added to reaction mixture followed by addition of 0.4 mM Na_2ATP to initiate the oxidation reaction. The vehicle control (0.1% DMSO), TG, TG + CPA or test compounds were introduced before the establishment of baseline. TG or TG + CPA were used as positive controls to determine SERCA1 and SERCA2-independent ATPase activity and verification of the assay system, respectively. To quantify the influence of SSd on SERCA activity, NADH oxidation rate (nmol/sec/mg protein) was calculated from epochs of 3 min and 5 min right after addition of Na_2ATP for SERCA1 and SERCA2, respectively.

2.9. Ca^{2+} imaging in HEK293 cells

Single-cell intracellular cytosolic Ca^{2+} was measured in null HEK293 or IP_3R triple knock out (KO) HEK293 cells stably expressing

Ca^{2+} indicator, GCaMP6m (Kovacevic et al., 2013). Ca^{2+} imaging was performed at room temperature using a ZEISS oberserver-Z1 microscope (Carl Zeiss AG, Jena, Germany). The imaging solution contained (in mM): NaCl 107, KCl 7.2, $MgCl_2$ 1.2, D-glucose 11.5, and HEPES 20 (pH 7.2). Fluorescence signals were recorded at a sampling rate of 2 Hz using an FITC filter. After recording the basal fluorescence for approximately 30 s, test compound was applied by bath perfusion and the signals were recorded for additional 600 s. Fluorescence data were presented as F/F_0. To quantify the influence of SSd on null HEK293 or IP_3R KO HEK293 cells, the AUC values were quantified from an epoch of 5 min right after addition of SSd.

2.10. Equilibrium [^{3}H]Ryanodine binding analysis

Equilibrium binding analyses of [^{3}H]Ryanodine ([^{3}H]Ry) to skeletal muscle RyR1 (0.05 mg/mL) and cardiac muscle RyR2 (0.5 mg/mL) were measured at 37 °C for 3 h with constantly shaking in a binding buffer containing (in mM): KCl 250, NaCl 14, HEPES 20, pH 7.4, and 2 μM free Ca^{2+} (obtained by the addition of EGTA calculated using software Bound-and-Determined (Brooks and Storey, 1992). The concentrations of [^{3}H]Ry were used at 1 nM and 2 nM for skeletal and cardiac preparations, respectively. Nonspecific [^{3}H]Ry binding was measured in the presence of 2 μM unlabeled ryanodine. Vesicles were harvested by rapid filtration through Whatman GF/B glass fiber filters (Whatman, Gaithersburg, MD, USA) using a 48-sample Cell Harvester (Brandel, Gaithersburg, MD, USA). Bound [^{3}H]Ry was quantified using a Beckman scintillation counter (Beckman, Indianapolis, IN, USA).

2.11. Single channel voltage clamp

Bilayer lipid membranes (BLM) were formed by mixing 30 mg/mL phosphatidylethanolamine, phosphatidylserine and phosphatidylcholine (lipid mixture) in n-decane. RyR1 channel incorporation into BLM was accomplished by induced vesicle fusions with BLM as previously described (Holland et al., 2017). Once channel fusion was successful, the recording buffer was adjusted to 500 mM (*cis*-cytoplasmic side) and 50 mM (*trans*-luminal side) CsCl, buffered with 20 mM HEPES, pH 7.4 to establish a 5:1 Cs^+ gradient. Fluctuations in channel current were recorded at a holding potential of −40 mV applied to the *trans* side adjusted to 100 μM Ca^{2+}. The Ca^{2+} in the *cis* side was 2 μM. Baseline was recorded for 1–1.5 min and extended for a time course of 3–15 min after addition of SSd. Data acquisition was made using digitizer DD1440 A (Axon-Molecular Devices), digitized at 10 kHz and filtered with 1 kHz low-pass filter (Low-Pass Bessel Filter 8 Pole). Data were quantified from a duration of 1 min after addition of SSd for 1 min. The parameters including channel open probability (P_o), mean open time (τ_o) and mean close time (τ_c) were performed using Clampfit 10.4 (Molecular Devices).

2.12. Calcein leak assay

Neocortical neurons cultured in 12-well plate at 7–9 DIV were used to examine the effect of SSd on the membrane permeability by measuring the leakage of calcein as described previously (Debiton et al., 2004; Gauthier et al., 2009). After loading with calcein-AM (5 μM) in Locke's buffer for 30 min at 37 °C, cells were exposed to SSd (3 μM). Media harvested at different time points were used to measure the fluorescence at 540 nm with excitation wavelength of 480 nm using a fluorescence microplate reader (Thermo Fisher Scientific, Waltham, MA, USA).

2.13. Measurement of Caspase-3 activity

Caspase-3 activity was determined by Caspase-3 activity assay kit (Nanjing Jiancheng Bioengineering Institute, Nanjing, Jiangsu, China). Briefly, cortical neurons at DIV 7–8 were lysed with lysis buffer provided by the kit, and lysate was centrifuged at 16,000 *g* for 15 min at 4 °C. The supernatant was collected for determining the protein concentration using BCA assay and measuring the activity of Caspase-3 according to the protocols provided by the manufactures.

2.14. Whole-cell voltage-clamp recording

Cultured neocortical neurons at 7–9 DIV were voltage-clamped by whole-cell patch-clamp using an EPC-10 amplifier and Pulse software (HEKA Elektronik, Lambrecht/Pfalz, Germany) as described previously (Paternain et al., 1996). Cells were bathed in extracellular solution containing (in mM): NaCl 140, KCl 5, D-glucose 10, $CaCl_2$ 2, $MgCl_2$ 1, HEPES 10, pH adjusted to 7.4 with NaOH. Pipettes were pulled from 1.5-mm capillary tubing and filled with intracellular solution containing (in mM): KCl 140, $CaCl_2$ 0.4, $MgCl_2$ 2, EGTA 1, HEPES 20, Na_2ATP 3, pH adjusted to 7.2 with KOH. Pipette-tip resistances were 2–3 MΩ. The cells were continuously clamped at a holding potential of −70 mV. Vehicle control (0.1% DMSO) and SSd were administrated by fast perfusion. Experimental data were collected and analyzed with Patchmaster (HEKA Elektronik) and Origin (version 8.0, OriginLab, Northampton, MA, USA).

2.15. Data analysis

Data analysis was performed using GraphPad Prism software (Version 5.0; GraphPad Software Inc., San Diego, CA, USA). Concentration-response relationship curves were fit by a non-linear regression equation with variable slope. Statistical significance was determined by One-way ANOVA analysis, where appropriate, a Dunnett's multiple comparison test or T- test; a p value below 0.05 was considered to be statistically significant.

3. Results

3.1. Influence of SSs on the cell viability in cultured neocortical neurons

The chemical structures of five SSs studied have been heuristically divided into two major classes depending on the presence (Type I: SSa, SSc and SSd) or absence (Type II: SSb1 and SSb2) of a cyclic ether linkage between C13 and C28 as illustrated in Fig. 1. Both SSa and SSd induced significant neocortical neuron death as reflected by the increase in PI positive neurons, enhanced formazan formation in MTT assay, and increased number of condensed nuclei (Fig. 2). The EC_{50} values for SSd induced neuronal death were 2.92 μM [1.14–5.74 μM, 95% confidence intervals (CI)], 2.56 μM (2.34–2.68, 95% CI), and 3.80 μM (1.92–7.53 μM, 95% CI) measured by the MTT assay (Fig. 2A), the FDA/PI double staining assay (Fig. 2B and C), and nuclei condensation assay (Fig. 2D), respectively. Consistent with its ability to induce nuclei condensation, SSd at 3 μM significantly increased Caspase-3 activity (Fig. 2E). SSa was ~ 5-fold less potent than SSd regardless of the neuronal death assay used, with EC_{50} values of 16.16 μM (13.55–19.26, 95% CI), 15.58 μM (13.76–17.64, 95% CI) and 14.49 μM (13.41–15.65 μM, 95% CI) in MTT, FDA/PI double staining and nuclei condensation assays, respectively. SSb1 appeared to be much less toxic, at the concentration of 30 μM, SSb1 only produced ~ 20% and 45% neuronal death in MTT and FDA/PI double staining assays, respectively (Fig. 2). The other two SSs, SSb2 and SSc, were without detectable effect on neuronal death with the assays tested in the present study (Fig. 2).

3.2. Influence of SSs on the $[Ca^{2+}]_i$ in cultured neocortical neurons

We next examined the influence of five SSs on the Ca^{2+} dynamics in neocortical neurons. Addition of SSa or SSd produced sustained elevation of $[Ca^{2+}]_i$ in a concentration-dependent manner with EC_{50} values of 8.1 μM (6.0–10.9 μM, 95% CI), or 2.9 μM (2.1–4.0 μM, 95% CI),

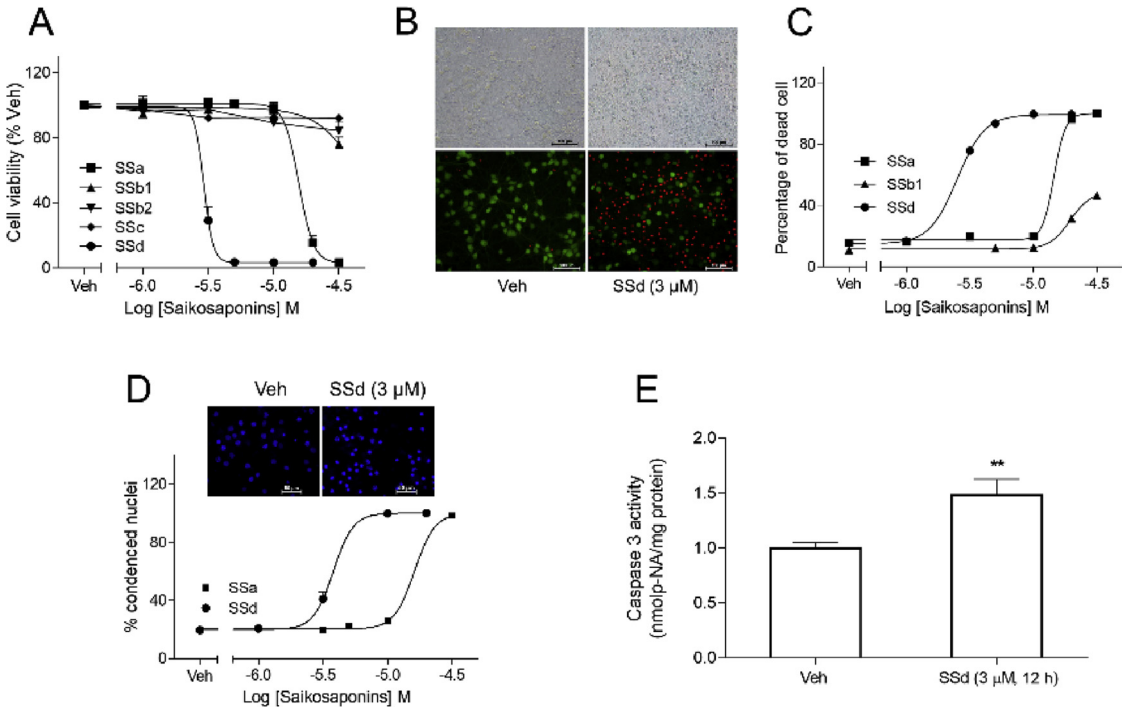

Fig. 2. SSs induce cell death in primary cultured neocortical neurons. (A) Concentration-response relationship curves for five SSs-induced neocortical neuronal cell death measured by formazan formation in MTT assay. (B) Representative images of FDA/PI labelled neocortical neurons treated with vehicle and SSd (3 μM). FDA in green; PI in red. (C) Concentration-response relationship curves for SSa-, SSb1-, and SSd-induced neuronal death quantified from FDA/PI staining. (D) Concentration-response relationship curves for SSa- and SSd-induced nuclei condensation visualized by Hoechst staining (Inlets are the representative images of Hoechst labelled nuclei treated with vehicle or 3 μM SSd). (E) SSd increased Caspase-3 activity. Each data point represents the Mean ± SEM from three independent experiments, each in five replicates. **, $p < 0.01$, SSd *vs.* Veh. Veh indicates 0.1% DMSO. (For interpretation of the references to colour in this figure legend, the reader is referred to the web version of this article.)

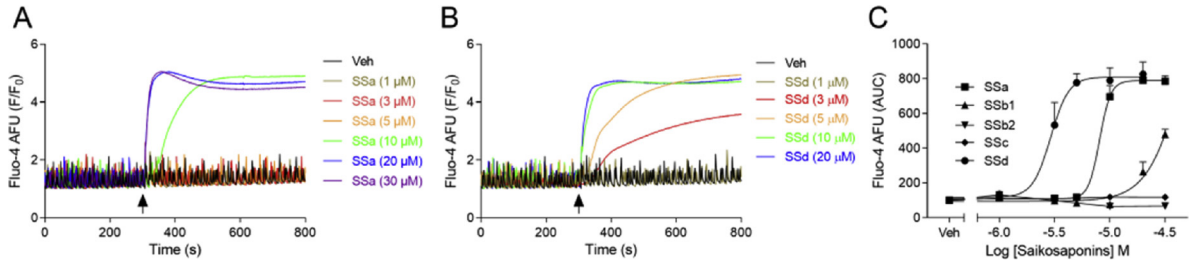

Fig. 3. SSs induce elevation in $[Ca^{2+}]_i$ in primary cultured neocortical neurons. SSa (A) and SSd (B) -induced $[Ca^{2+}]_i$ elevation in neocortical neurons as a function of time. (C) Concentration-response relationship curves for SSs-elevated $[Ca^{2+}]_i$. Each data point represents the Mean ± SEM from three independent experiments, each in six replicates. Arrow indicates the addition of Veh or test compounds. Veh indicates 0.1% DMSO.

respectively (Fig. 3A and B). The rise in $[Ca^{2+}]_i$ with SSb1 addition was only detectable at concentrations ≥ 20 μM, suggesting that SSb1 was much less potent (Fig. 3C). SSb2 and SSc were inactive on the $[Ca^{2+}]_i$ overloading up to 30 μM (Fig. 3C).

3.3. SSd triggered Ca^{2+} release from microsomal vesicles

The increase in neuronal cytoplasmic $[Ca^{2+}]_i$ could result from enhanced Ca^{2+} entry across the plasma membrane, release of intracellular Ca^{2+} stores, or both. We therefore tested whether SSd triggers the release of Ca^{2+} from microsomal vesicles in the presence of active SERCA pump activity. After Ca^{2+} was loaded into the vesicles by three bolus sequential additions of extravesicular Ca^{2+}, addition of SSd elicited release of Ca^{2+} from the vesicles in a concentration-dependent manner. SERCA inhibitor TG (30 μM) also produced Ca^{2+} release from the vesicles although the maximum rate of release was ~ 11-fold smaller than SSd (10 μM) (Fig. 4).

3.4. SSd negligibly inhibited SERCA activity

Virtual ligand docking studies and coupled enzyme assay have suggested that SSd may cause $[Ca^{2+}]_i$ overloading by suppressing SERCA activity (Wong et al., 2013). We therefore investigated whether SSd can directly suppress SERCA activity. Coupled enzyme assay was used to evaluate the inhibitory effect of SSd on SERCA activity. In contrast to previous published results we found that even at as high as 30 μM SSd only negligibly suppressed SERCA1 (~ 9.8% inhibition) and SERCA2 (~17.6% inhibition) activity (Fig. 5).

3.5. RyR only partially contributes to SSd-induced Ca^{2+} release

Given the massive Ca^{2+} release from JSR vesicle flux model, we next investigated whether Ca^{2+}-releasing channels were engaged in SSd-induced Ca^{2+} release. In the presence of RR, which suppresses RyR but not inositol trisphosphate receptor (IP_3R) function, SSd-triggered efflux rate was inhibited by ~ 59% in the presence of RR after release

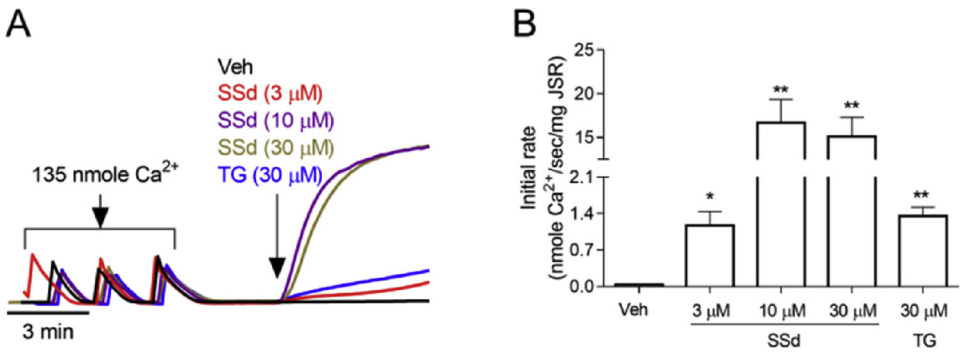

Fig. 4. Effects of SSd on calcium release in junctional sarcoplasmic reticulum (JSR) microsomal preparation. (A) Representative traces of Ca^{2+} fluxes from JSR, a total of 135 nmole Ca^{2+} was sequentially loaded to the vesicles. 2–3 min following the accumulation of final bolus of $CaCl_2$ was completed, Veh or appropriate concentration of SSd was added to the system. (B) Quantification of Ca^{2+} release rate from the initial 60 s upon the introduction of SSd. *, $p < 0.05$, **, $p < 0.01$, Drugs *vs.* Veh. Thapsigargin (TG, 30 μM) was used as a positive control. Each data point represents the Mean ± SEM (n = 5). Arrow indicates the addition of compounds. Veh indicates 0.1% DMSO.

was initiated (Fig. 6A and B). Equilibrium [^{3}H]Ry binding analysis demonstrated that SSd increased [^{3}H]Ry binding to JSR vesicles (RyR1) at concentrations greater than 3 μM but had no measurable influence on cardiac ventricle homogenate preparations (RyR2) (Fig. 6C). The EC_{50} value for SSd-evoked increase in [^{3}H]Ry binding to RyR1 was 18.1 μM (13.9–30.1 μM, 95% CI) and the maximal increase reached 290% of control (Fig. 6C). In lipid bilayer single channel recording, SSd (1 μM) significantly increased RyR 1 channel activity by increasing the channel open probability (Po), the mean open time (τ_o) as well as by decreasing the mean close time (τ_c) (Fig. 6D and E). To investigate the effect of SSd on IP_3R, SSd-induced Ca^{2+} response was investigated in null HEK293 cells and IP_3R triple KO HEK293 cells. SSd (3 μM) induced similar Ca^{2+} response between these cells excluding activation of IP_3R by SSd (Fig. 6F and G). Similarly, a phospholipase C inhibitor, U73122 (3 μM), failed to prevent SSd (3 μM)-induced Ca^{2+} overloading in neocortical neurons, which further excluded the engagement of PLC-IP_3R pathway on SSd-induced elevation of $[Ca^{2+}]_i$ (Fig. 6H).

3.6. SSd-induced $[Ca^{2+}]_i$ overload in primary neurons independent of Ca^{2+} release from intracellular Ca^{2+} store

Given the direct but weak activation of RyR by SSd, we next investigated whether SSd-induced Ca^{2+} release in JSR vesicle translated into endoplasmic reticulum (ER) store depletion in intact neurons. Neocortical neurons were treated with 10 μM TG for 50 min to deplete the intracellular Ca^{2+} store and then were challenged with 3 μM SSd. Depletion of intracellular Ca^{2+} store had no effect on the rise in $[Ca^{2+}]_i$ triggered by SSd (3 μM), thereby excluding Ca^{2+} release from ER/sarcoplasmic reticulum (SR) Ca^{2+} store as the primary source for SSd-elevated $[Ca^{2+}]_i$ in intact neocortical neurons (Fig. 7A and B)

3.7. SSd-induced $[Ca^{2+}]_i$ overloading was dependent on extracellular Ca^{2+} influx

Given the lack of detectable influence of ER Ca^{2+} store depletion on SSd-induced $[Ca^{2+}]_i$ rise, we investigated whether the rise in $[Ca^{2+}]_i$ in neocortical neurons was partially or wholly dependent on influx of extracellular Ca^{2+}. After loading the Ca^{2+} fluorescence dye, Fluo-4/AM, the cells were bathed in normal (2.3 mM), medium (0.2 mM) and 0 mM Ca^{2+} (chelated with 1 mM EGTA) Locke's buffer. Lower extracellular Ca^{2+} concentration significantly attenuated SSd-induced Ca^{2+} response observed in the physiological buffer (Fig. 8A and B).

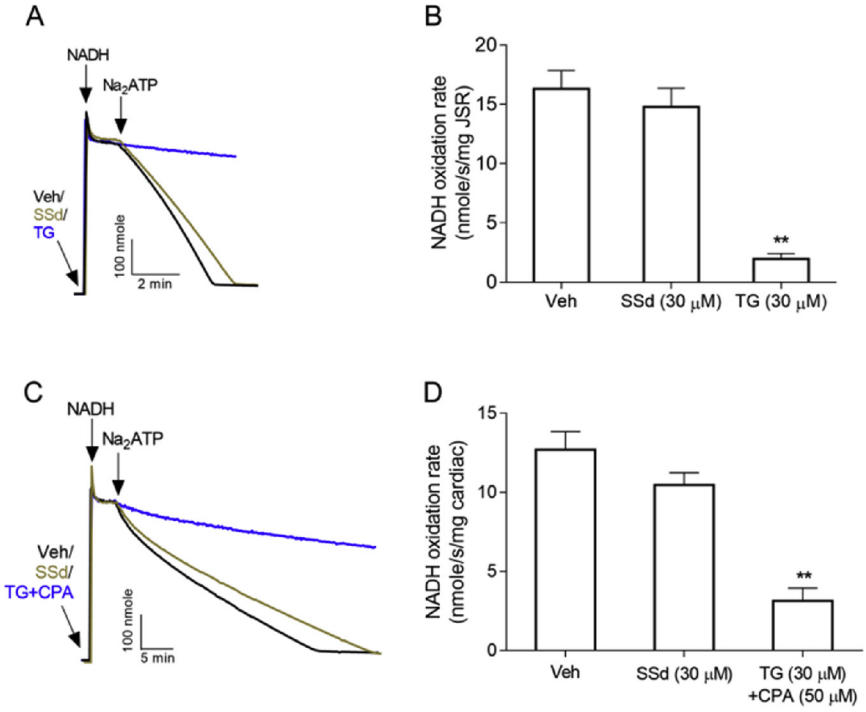

Fig. 5. Lack of effect of SSd on SERCA1 and SERCA2 activities. (A) Representative oxidation traces of NADH in coupled enzyme assay were monitored by measuring absorbance at 340–400 nm. Test compounds or Veh was added separately to each cuvettes followed by the addition of NADH and Na_2ATP to initiate the reaction. TG (30 μM) was used as a positive control. (B) Quantification of NADH oxidation rate in the absence and presence of SSd. **, $p < 0.01$, TG *vs.* Veh. (C) Time-response relationship of SSd on SERCA2 activity in heart ventricle homogenate. TG + cyclopiazonic acid (CPA) was used as a positive control. (D) Quantification of NADH oxidation rate in the absence and presence of SSd. Each data point represents the Mean ± SEM (n = 3). **, $p < 0.01$, TG + CPA *vs.* Veh. Veh indicates 0.1% DMSO.

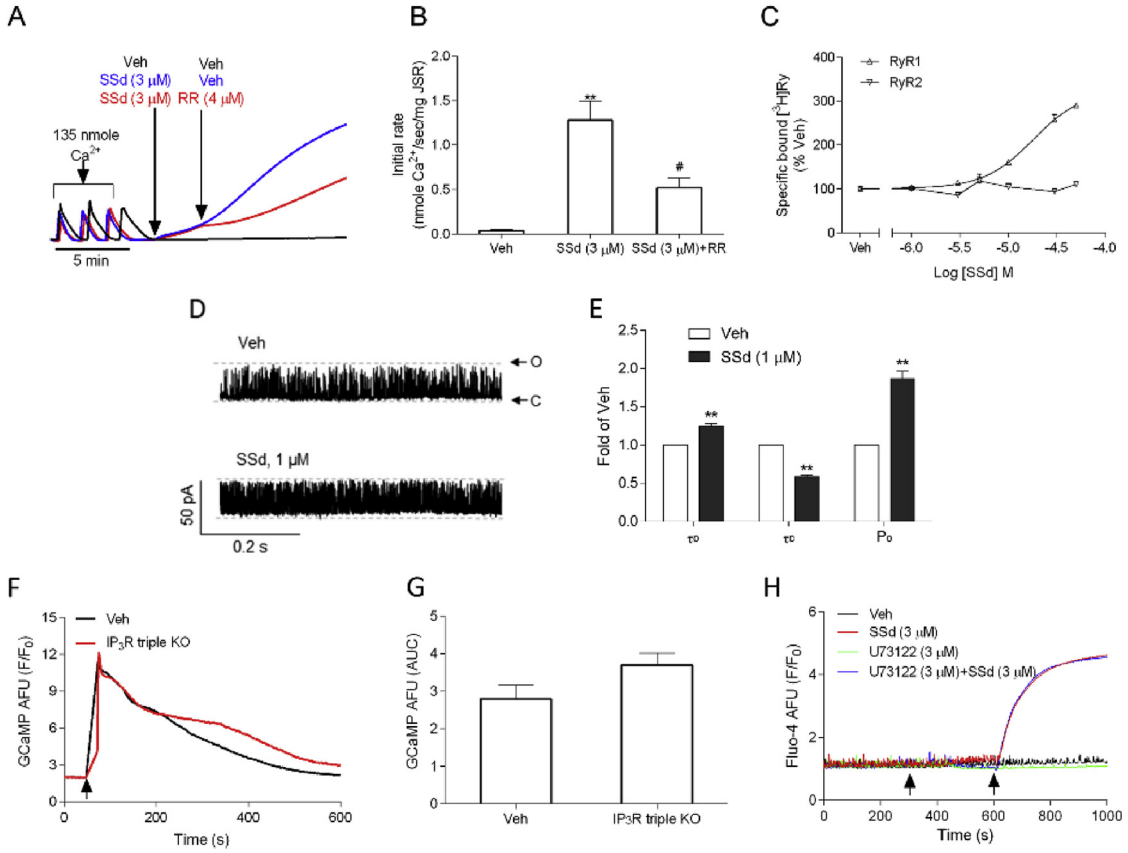

Fig. 6. SSd directly activates ryanodine receptor. (A) Time-response relationship for ruthenium red (RR, 4 μM) on SSd-stimulated Ca^{2+} release in JSR. (B) Quantification of RR effect on SSd-stimulated Ca^{2+} release. **, $p < 0.01$, SSd *vs.* Veh; $^{\#}$, $p < 0.05$, SSd + RR *vs.* SSd (n = 3). (C) Concentration-response curves to SSd linked by line showing [^{3}H]Ryanodine ([^{3}H]Ry) binding to RyR1 and RyR2. All the data points were normalized to the mean value of Veh group. (D) Representative traces of RyR1 channel activity in lipid bilayer single channel recording in the absence and presence of 1 μM SSd. (E) Quantification of SSd (1 μM) on RyR1 channel gating parameters including channel open probability (P_o), mean open time (τ_o) and mean close time (τ_c). Each data point represents the Mean ± SEM from 3 independent channels. Statistical significance between groups was calculated by T-test. **, $p < 0.01$, SSd *vs.* Veh. (F) Representative traces of SSd-stimulated $[Ca^{2+}]_i$ changes in null HEK293 and IP_3R triple KO HEK293 cells as a function of time. Arrow indicates the addition of SSd (3 μM). (G) Quantification of SSd-stimulated $[Ca^{2+}]_i$ overloading in null HEK293 and IP_3R triple KO HEK293 cells (n = 6). The area under curve (AUC) values were calculated from an epoch of 5 min after addition of SSd. (H) Influence of U73122 (3 μM) on SSd-stimulated $[Ca^{2+}]_i$ elevation. The first arrow indicates the addition of Veh or U73122 and the second arrow indicates the addition of Veh or SSd (3 μM). Veh indicates 0.1% DMSO.

3.8. SSd-induced elevation in $[Ca^{2+}]_i$ was not dependent on the major routes of Ca^{2+} influx

Given the involvement of extracellular Ca^{2+} influx on SSd-elevated $[Ca^{2+}]_i$, we next investigated whether known inhibitors/blockers of Ca^{2+} regulatory proteins expressed and targeted to plasma membrane of neurons were potential targets of SSd. Inhibitors tested included nifedipine, an inhibitor of L-type calcium channels, KB-R7943, an antagonist of Na^+-Ca^{2+} exchanger, MK-801, an inhibitor of NMDAR, CNQX, an α-amino-3-hydroxy-5-methyl-4-isoxazolepropionic acid receptor/kainic acid receptor (AMPAR/KAR) inhibitor, SB366791, a TRPV1 inhibitor, and RR, a non-selective cation channel blocker. However, none of these inhibitors was effective in mitigating SSd-elevated $[Ca^{2+}]_i$ in neocortical neurons (Fig. 9).

3.9. SSd enhanced membrane permeability in primary cultured neocortical neurons

Given that the SSd-triggered increase in $[Ca^{2+}]_i$ seemed non-selective, we more closely examined actions of SSd on the plasma membrane. After loaded with calcein-AM, neurons were washed and exposed to vehicle control (0.1% DMSO) or SSd and the temporal release of calcein was measured. SSd produced a significant efflux of calcein at as early as 8 min post-exposure, which continued to gradually increase

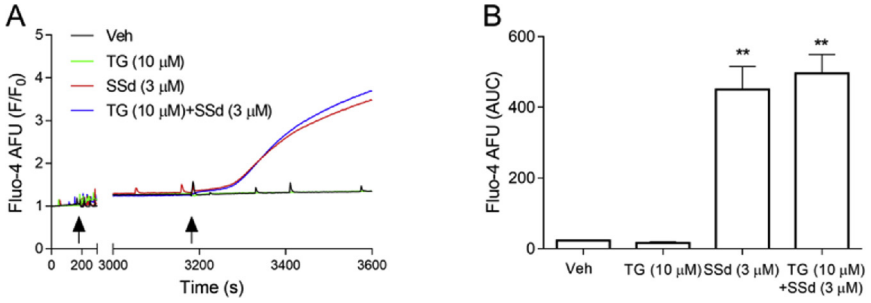

Fig. 7. Depletion of intracellular Ca^{2+} store by TG (10 μM) did not affect SSd (3 μM)-induced $[Ca^{2+}]_i$ increase. (A) Representative traces of SSd-stimulated $[Ca^{2+}]_i$ elevation in the absence and presence of TG. The first arrow indicates the addition of Veh or TG, and the second arrow indicates the addition of Veh or SSd (3 μM). (B) Quantification of TG effect on SSd-induced $[Ca^{2+}]_i$ overloading. The area under curve (AUC) values were obtained from an epoch of 5 min after second addition. **, $p < 0.01$, Drugs *vs.* Veh. Each data point represents the Mean ± SEM from three independent cultures, each in triplicates. Veh indicates 0.1% DMSO.

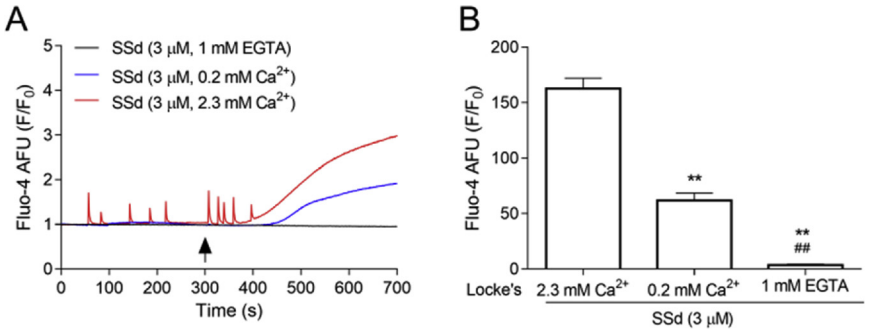

Fig. 8. SSd-induced $[Ca^{2+}]_i$ increase is dependent on the extracellular Ca^{2+} influx. (A) Representative traces of SSd-elevated $[Ca^{2+}]_i$ as a function of time in 2.3 mM, 0.2 mM, and 0 mM Ca^{2+} buffers (containing 1 mM EGTA). Arrow indicates addition of SSd (3 μM). (B) Quantification of SSd Ca^{2+} response in 2.3 mM, 0.2 mM, and 0 mM Ca^{2+} buffers (containing 1 mM EGTA). The area under curve (AUC) values were obtained from an epoch of 5 min addition of SSd. **, $p < 0.01$, 0 mM or 0.2 mM Ca^{2+} *vs.* 2.3 mM Ca^{2+}; $^{\#\#}$, $p < 0.01$, 0 mM Ca^{2+} *vs.* 0.2 mM Ca^{2+}. Each data point represents the Mean ± SEM from three independent cultures, each in triplicates. Veh indicates 0.1% DMSO.

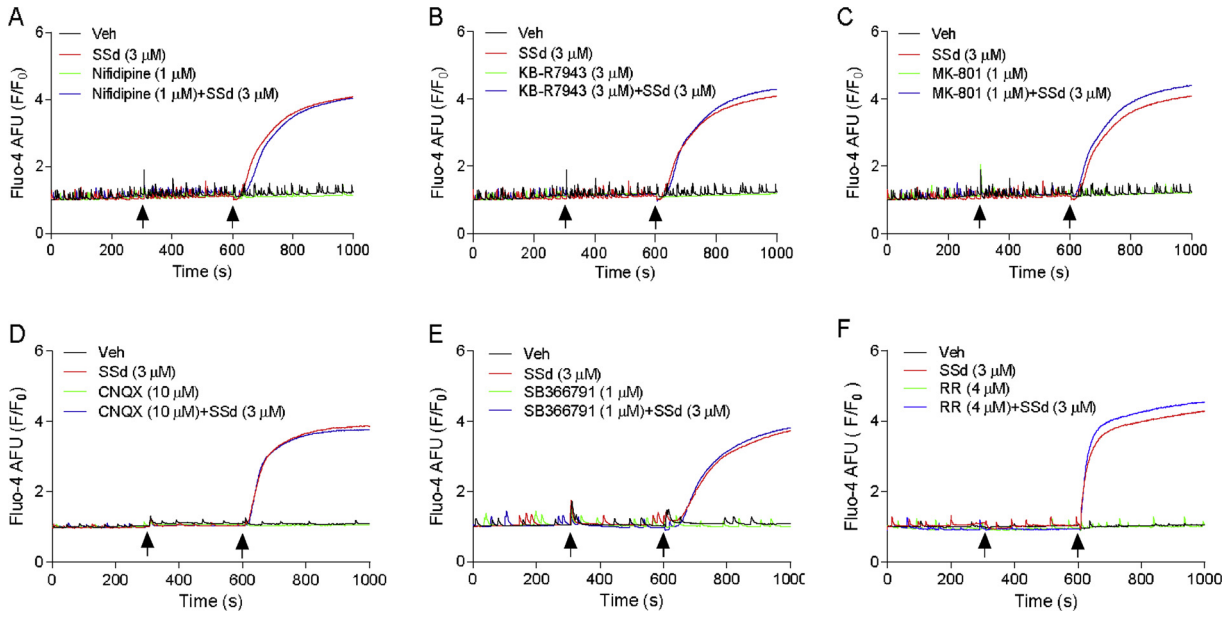

Fig. 9. Major Ca^{2+} influx routes are not involved in SSd-elevated $[Ca^{2+}]_i$. Representative traces of nifedipine (A), KB-R7943 (B), MK-801 (C), CNQX (D), SB366791 (E), and RR (F) effect on SSd-stimulated $[Ca^{2+}]_i$ elevation as a function of time. This experiment was performed in three independent cultures, each in triplicates with similar results. The first arrow indicates the addition of Veh or inhibitor and the second arrow indicates the addition of Veh or SSd (3 μM). Veh indicates 0.1% DMSO.

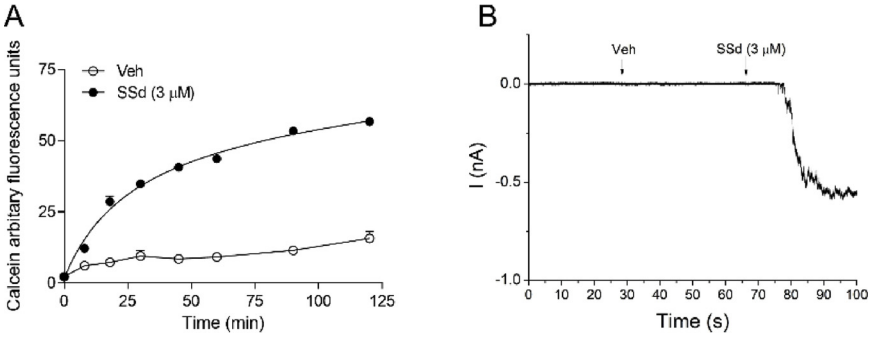

Fig. 10. SSd increases membrane permeability in cultured neocortical neurons. (A) SSd (3 μM)-induced calcein efflux in neocortical neurons as a function of time. Each data point represents the Mean ± SEM from three independent cultures, each in triplicates. (B) Representative trace of SSd-induced inward current. The first arrowhead indicates the addition of Veh and the second arrowhead indicates the addition of SSd (3μM) perfusion. This experiment was performed in 5 neocortical neurons with similar results. Veh indicates 0.1% DMSO.

and saturated over 90 min (Fig. 10A). To further examine the membrane effect, neocortical neurons were voltage-clamped at a holding potential of −70 mV. Addition of SSd (3 μM) but not vehicle (0.1% DMSO) induced an inward current (Fig. 10B).

4. Discussion

As one of the main anti-fever and anti-inflammation traditional Chinese medicines used in the clinic, preparations of Radix bupleuri have been reported to display severe side effects in many organ systems (Itoh et al., 1995; Lee et al., 2011; Li et al., 2017c; Xu et al., 2018). Clinical safety issues have prompted the China Food and Drug Administration to require a black box warning for products containing Radix bupleuri. Recent studies have demonstrated that SSd suppresses mouse motor activity, impairs learning and memory, and decreases hippocampal neurogenesis (Xu et al., 2018). In the present study we demonstrate that SSa, SSb1 and SSd induce neurotoxicity in primary cultured neocortical neurons with rank order of SSd > SSa > SSb1, whereas SSb2 and SSc have no significant effect on the cell viability of neocortical neurons. The rank order of SSs on neurotoxicity is consistent with their hemolytic and anti-inflammatory activity, as well as their inhibitory action on drug-induced hepatic injury (Abe et al., 1981b; Ashour and Wink, 2011; Yuan et al., 2017). SSa and SSd produce significant neurotoxicity while SSb1 is much less toxic and SSb2 is

without toxic effect on the neocortical neurons, suggesting the importance of the cyclic ether linkage between C13 and C28. In addition, the conformation of the hydroxyl group at C16 also appears to be important for SS-induced neurotoxicity.

Previous studies have demonstrated that SSd elevated $[Ca^{2+}]_i$ level in Hela and MCF-7 cells and this elevated $[Ca^{2+}]_i$ level was responsible for the autophagic cell death, posited to be mediated by over-activation of the Ca^{2+}/calmodulin-dependent kinase kinase-AMP-activated protein kinase-mammalian target of rapamycin (CaMKK-AMPK-mTOR) pathway (Wong et al., 2013). Tight spatial and temporal regulation of $[Ca^{2+}]_i$ levels controls neuronal development, including activity-dependent neurite outgrowth and synaptogenesis, whereas uncontrolled changes in $[Ca^{2+}]_i$ lead to neuronal death (George et al., 2012; He et al., 2017; Zieminska et al., 2017). Here we demonstrate that SSs trigger robust elevation of $[Ca^{2+}]_i$ in neocortical neurons. The ability of SSs to elevate $[Ca^{2+}]_i$ parallels its acute neurotoxicity with respect to potency.

Previous studies have suggested that SSd is a SERCA inhibitor and responsible for elevated $[Ca^{2+}]_i$ in Hela and MCF-7 cancer cells, as well as cardiomyocytes and hepatocytes (Wang et al., 2017; Wong et al., 2013). However, the significant differences between SSd concentrations needed to influence $[Ca^{2+}]_i$ and those needed to inhibit SERCA make it unlikely that SERCA inhibition is a primary mechanism leading to the rise in $[Ca^{2+}]_i$ and loss of cell viability. SSd at 10 μM produced a robust $[Ca^{2+}]_i$ elevation in Hela and MCF-7 cells but had negligible inhibition of SERCA activity (~ 15% inhibition) (Wong et al., 2013), consistent with our data that indicated SSd at 30 μM minimally suppressed SERCA1 (~ 10%) and SERCA2 (~ 18%). Although RyR1, but not RyR2, appeared to represent a direct target of SSd in equilibrium [^{3}H] Ry binding assays and single channel recording, direct activation of RyR1 by SSd may be only partially responsible for Ca^{2+} efflux from JSR vesicle preparations since release was only partially suppressed by RR, a potent and complete blocker of RyR1-mediated Ca^{2+} release (Mack et al., 1992; Xu et al., 1998).

Our results showed that SSd-triggered elevation of $[Ca^{2+}]_i$ was primarily mediated through the entry of extracellular Ca^{2+} in intact neocortical neurons. Depletion of Ca^{2+} stores with TG (10 μM) did not mitigate the influences of SSd on $[Ca^{2+}]_i$ suggesting that depletion of the intracellular Ca^{2+} store was not a necessary step for SSd-elevated $[Ca^{2+}]_i$. Moreover, lower the extracellular Ca^{2+} concentrations proportionally reduced SSd Ca^{2+} response suggesting the major role of extracellular Ca^{2+} influx for SSd-elevated $[Ca^{2+}]_i$.

SSd-induced Ca^{2+} influx was not attenuated by addition of several blockers of major neuronal Ca^{2+} entry pathways, including L-type Ca^{2+} channels, NMDAR, AMPAR, Na^+-Ca^{2+} exchanger, and TRPV1. These data suggest that SSd acts though a non-selective mechanism, possibly as a potent Ca^{2+} ionophore. A nonselective ionophore mechanism is consistent with previous results showing that SSs caused a significant decrease in the negative charge on the cell surface and the destruction of microvilli (Abe et al., 1981a). Saponins are, in fact, amphiphilic molecules possessing a lipophilic aglycone and a hydrophilic sugar side chain. Digitonin, a steroidal saponin disintegrates biological and artificial membranes, increases membrane permeability and causes membrane rupturing which is dependent on the presence of cholesterol (Sudji et al., 2015). In addition to steroidal saponins, avicins, a class of triterpenoid saponins with structural similarities to SSd, have been shown to form non-selective cation/anion channels with an estimated pore size of 1.1 nm in radius (Li et al., 2005). Considered together, these data strongly suggest that SSd-increased $[Ca^{2+}]_i$ is likely mediated through incorporation of ionophore that enhances Ca^{2+} influx. This interpretation is further supported by calcein efflux and patch-clamp recording experiments in which SSd produces a significant efflux of calcein and an inward current in neocortical neurons. Intercalation of SSd with the plasma membrane most likely accounts for its potent cytotoxicity towards various cancer cells, as well as primary cells in culture (Li et al., 2017b; Wong et al., 2013; Yao et al., 2014; Zhong et al., 2016). The mechanism of how SSd increases the membrane permeability and whether it possesses ion selectivity need further exploration. In addition, whether SSd neuronal toxicity is solely dependent on increased $[Ca^{2+}]_i$ needs further investigation.

In summary, we demonstrate that SSd induces apoptotic neuronal death in primary cultured neocortical neurons. This neuronal death is parallel to massive extracellular Ca^{2+} influx as a consequence to the enhanced membrane permeability, most likely by interacting with membrane bilayers to form pores permeable to Ca^{2+}.

Conflict of interest statement

The authors declare no conflicts of interest.

Transparency document

The Transparency document associated with this article can be found in the online version.

Acknowledgments

This work was supported by National Natural Science Foundation of China (No. 21777192, 81473539); National Key R&D program of China (No. 2018YFF0215200); National Science and Technology Major Projects for “Major New Drugs Innovation and Development” (2018ZX09101003-004-002); “111”” project (B16046) from the Ministry of Education of China and the State Administration of Foreign Experts Affairs of China. This work was also supported by the National Institutes of Health (NIH) (R01 ES014901, P01 AR052354, P01 ES011269, P42 ES04699), and the US Environmental Protection Agency (STARR829388 and R833292).

References

Abe, H., et al., 1981a. Effects of saikosaponins on biological membranes. 3. Ultrastructural studies on effects of saikosaponins on the cell surface. Planta Med. 42 (4), 356–363.
Abe, H., et al., 1981b. Erythrocyte membrane stabilization by plant saponins and sapogenins. Naunyn Schmiedebergs Arch Pharmacol 316 (3), 262–265.
Ashour, M.L., Wink, M., 2011. Genus Bupleurum: a review of its phytochemistry, pharmacology and modes of action. J. Pharm. Pharmacol. 63 (3), 305–321.
Brooks, S.P., Storey, K.B., 1992. Bound and determined: a computer program for making buffers of defined ion concentrations. Anal. Biochem. 201 (1), 119–126.
Cao, Z., et al., 2010. Involvement of caspase activation in azaspiracid-induced neurotoxicity in neocortical neurons. Toxicol. Sci. 114 (2), 323–334.
Cao, Z., et al., 2014. Nanomolar bifenthrin alters synchronous Ca2+ oscillations and cortical neuron development independent of sodium channel activity. Mol. Pharmacol. 85 (4), 630–639.
Cao, Z., et al., 2015. Rapid throughput analysis demonstrates that chemicals with distinct seizurogenic mechanisms differentially alter Ca2+ dynamics in networks formed by hippocampal neurons in culture. Mol. Pharmacol. 87 (4), 595–605.
Chen, L., et al., 2013. Saikosaponin D disrupts platelet-derived growth factor-beta receptor/p38 pathway leading to mitochondrial apoptosis in human LO2 hepatocyte cells: a potential mechanism of hepatotoxicity. Chem-Biol Interact 206 (1), 76–82.
Chen, M., et al., 2016. Saikosaponin d induces cell death through caspase-3-dependent, caspase-3-independent and mitochondrial pathways in mammalian hepatic stellate cells. BMC Cancer 16, 532.
Cherednichenko, G., et al., 2004. NADH oxidase activity of rat cardiac sarcoplasmic reticulum regulates calcium-induced calcium release. Circ. Res. 94 (4), 478–486.
Debiton, E., et al., 2004. In addition to membrane injury, an affinity for melanin might be involved in the high sensitivity of human melanoma cells to hederacolchiside A1. Melanoma Res. 14 (2), 97–105.
Du, Z., et al., 2018. Saikosaponin a ameliorates LPS-Induced acute lung injury in mice. Inflammation 41 (1), 193–198.
Fang, W., et al., 2017. Anti-influenza triterpenoid saponins (saikosaponins) from the roots of Bupleurum marginatum var. stenophyllum. Bioorg Med Chem Lett 27 (8), 1654–1659.
Feng, W., et al., 2017. Enantioselectivity of 2,2',3,5',6-pentachlorobiphenyl (PCB 95) atropisomers toward ryanodine receptors (RyRs) and their influences on hippocampal neuronal networks. Environ. Sci. Technol. 51 (24), 14406–14416.
Fu, Y., et al., 2015. Saikosaponin a inhibits lipopolysaccharide-oxidative stress and inflammation in Human umbilical vein endothelial cells via preventing TLR4 translocation into lipid rafts. Free Radic. Biol. Med. 89, 777–785.
Gao, W., et al., 2017. SSa ameliorates the Glu uptaking capacity of astrocytes in epilepsy via AP-1/miR-155/GLAST. Biochem. Biophys. Res. Commun. 493 (3), 1329–1335.

Gauthier, C., et al., 2009. Haemolytic activity, cytotoxicity and membrane cell permeabilization of semi-synthetic and natural lupane- and oleanane-type saponins. Bioorg. Med. Chem. 17 (5), 2002–2008.
George, J., et al., 2012. Bidirectional influence of sodium channel activation on NMDA receptor-dependent cerebrocortical neuron structural plasticity. P Natl Acad Sci USA 109 (48), 19840–19845.
He, Y., et al., 2017. Activation of sodium channels by alpha-scorpion toxin, BmK NT1, produced neurotoxicity in cerebellar granule cells: an association with intracellular Ca(2+) overloading. Arch. Toxicol. 91 (2), 935–948.
Holland, E.B., et al., 2017. An extended structure-activity relationship of Nondioxin-like PCBs evaluates and supports modeling predictions and identifies picomolar potency of PCB 202 towards Ryanodine receptors. Toxicol. Sci. 155 (1), 170–181.
Ikegami, F., et al., 2006. Pharmacology and toxicology of Bupleurum root-containing Kampo medicines in clinical use. Hum. Exp. Toxicol. 25 (8), 481–494.
Itoh, S., et al., 1995. Liver injuries induced by herbal medicine, syo-saiko-to (xiao-chai-hu-tang). Dig. Dis. Sci. 40 (8), 1845–1848.
Kovacevic, I., et al., 2013. Filamin and phospholipase C-epsilon are required for calcium signaling in the Caenorhabditis elegans spermatheca. PLoS Genet. 9 (5), e1003510.
Lee, C., et al., 2011. Risk of liver injury associated with Chinese herbal products containing Radix bupleuri in 639,779 patients with hepatitis B virus infection. PLoS One 6 (1), e16064.
Levitz, S.M., Diamond, R.D., 1985. A rapid colorimetric assay of fungal viability with the tetrazolium salt MTT. J. Infect. Dis. 152 (5), 938–945.
Li, X., et al., 2005. Proapoptotic triterpene electrophiles (avicins) form channels in membranes: cholesterol dependence. Biophys. J. 88 (4), 2577–2584.
Li, Y., et al., 2017. Saikosaponin D relieves unpredictable chronicmild stress induced depressive-like behavior in rats: involvement of HPA axisand hippocampal neurogenesis. Psychopharmacology 234, 3385–3394.
Li, C., et al., 2017a. Reversal of P-glycoprotein-mediated multidrug resistance is induced by saikosaponin D in breast cancer MCF-7/adriamycin cells. Pathol. Res. Pract. 213 (7), 848–853.
Li, C., et al., 2017b. The effect of saikosaponin D on doxorubicin pharmacokinetics and its MDR reversal in MCF-7/adr cell xenografts. Eur. Rev. Med. Pharmacol. Sci. 21 (19), 4437–4445.
Li, X., et al., 2017c. Saikosaponins induced hepatotoxicity in mice via lipid metabolism dysregulation and oxidative stress: a proteomic study. BMC Complement. Altern. Med. 17 (1), 219.
Liu, A., et al., 2014. Saikosaponin d protects against acetaminophen-induced hepatotoxicity by inhibiting NF-kappaB and STAT3 signaling. Chem-Biol Interact 223, 80–86.
Lu, C.N., et al., 2012. Saikosaponin a and its epimer saikosaponin d exhibit anti-inflammatory activity by suppressing activation of NF-kappaB signaling pathway. Int. Immunopharmacol. 14 (1), 121–126.
Ma, X., et al., 2015. Saikosaponin-D reduces cisplatin-induced nephrotoxicity by repressing ROS-mediated activation of MAPK and NF-kappaB signalling pathways. Int. Immunopharmacol. 28 (1), 399–408.
Maccioni, P., et al., 2016. Reducing effect of saikosaponin A, an active ingredient of Bupleurum falcatum, on alcohol self-administration in rats: possible involvement of the GABAB receptor. Neurosci. Lett. 621, 62–67.
Mack, W.M., et al., 1992. Discrimination of multiple binding sites for antagonists of the calcium release channel complex of skeletal and cardiac sarcoplasmic reticulum. J. Pharmacol. Exp. Ther. 262 (3), 1028–1037.
National Pharmacopoeia Committee NP, 2015. China Pharmacopoeia. Pharmacopoeia of People' S Republic of China. Chemical Industry Press, Beijing, pp. 280 vol Part one.
Nayler, W.G., 1983. Calcium and cell death. Eur. Heart J. 4 (Suppl C), 33–41.
Paternain, A.V., et al., 1996. Comparative antagonism of kainate-activated kainate and AMPA receptors in hippocampal neurons. Eur. J. Neurosci. 8 (10), 2129–2136.
Pessah, I.N., et al., 1986. Calcium-ryanodine receptor complex. Solubilization and partial characterization from skeletal muscle junctional sarcoplasmic reticulum vesicles. J. Biol. Chem. 261 (19), 8643–8648.
Saneyoshi, T., et al., 2008. Activity-dependent synaptogenesis: regulation by a CaM-kinase kinase/CaM-kinase I/betaPIX signaling complex. Neuron 57 (1), 94–107.
Smutny, T., et al., 2018. A feasibility study of the toxic responses of human induced pluripotent stem cell-derived hepatocytes to phytochemicals. Toxicol. In Vitro 52, 94–105.
Sudji, I.R., et al., 2015. Membrane disintegration caused by the steroid saponin digitonin is related to the presence of cholesterol. Molecules 20 (11), 20146–20160.
TA, Ta, et al., 2006. Hydroxylated xestospongins block inositol-1,4,5-trisphosphate-induced Ca2+ release and sensitize Ca2+-induced Ca2+ release mediated by ryanodine receptors. Mol. Pharmacol. 69 (2), 532–538.
Wang, S., et al., 2017. Content decline of SERCA inhibitors saikosaponin a and d attenuates cardiotoxicity and hepatotoxicity of vinegar-baked Radix bupleuri. Environ Toxicol Phar 52, 129–137.
Wang, J., et al., 2018. Saikosaponin a inhibits LPS-Induced endometritis in mice through activating Nrf2 signaling pathway. Inflammation 41 (4), 1508–1514.
Wong, V.K., et al., 2013. Saikosaponin-d, a novel SERCA inhibitor, induces autophagic cell death in apoptosis-defective cells. Cell Death Dis. 4, e720.
Xie, W., et al., 2013. Saikosaponin a enhances transient inactivating potassium current in rat hippocampal CA1 neurons. Evid-based Compl Alt 2013, 413092.
Xu, L., et al., 1998. Potential for pharmacology of ryanodine receptor/calcium release channels. Ann NY Acad Sci 853, 130–148.
Xu, L., et al., 2018. Saikosaponin-d-mediated downregulation of neurogenesis results in cognitive dysfunction by inhibiting Akt/Foxg-1 pathway in mice. Toxicol. Lett. 284, 79–85.
Yang, F., et al., 2017. Radix bupleuri: a review of traditional uses, botany, phytochemistry, pharmacology, and toxicology. Biomed Res. Int. 2017, 7597596.
Yao, M., et al., 2014. Saikosaponin-d inhibits proliferation of DU145 human prostate cancer cells by inducing apoptosis and arresting the cell cycle at G0/G1 phase. Mol. Med. Rep. 10 (1), 365–372.
Ye, M., et al., 2016. Saikosaponin a functions as anti-epileptic effect in pentylenetetrazol induced rats through inhibiting mTOR signaling pathway. Biomed. Pharmacother. 81, 281–287.
Yoon, S.S., et al., 2012. Effect of saikosaponin A on maintenance of intravenous morphine self-administration. Neurosci. Lett. 529 (1), 97–101.
Yoon, S.S., et al., 2013. Effects of saikosaponin A on cocaine self-administration in rats. Neurosci. Lett. 555, 198–202.
Yu, Y., et al., 2012. Saikosaponin a mediates the anticonvulsant properties in the HNC models of AE and SE by inhibiting NMDA receptor current and persistent sodium current. PLoS One 7 (11), e50694.
Yuan, B., et al., 2017. A systematic review of the active saikosaponins and extracts isolated from Radix bupleuri and their applications. Pharm Biol 55 (1), 620–635.
Zhang, F., et al., 2016. Activation of Fas death receptor pathway and Bid in hepatocytes is involved in saikosaponin D induction of hepatotoxicity. Environ Toxicol Phar 41, 8–13.
Zhong, D., et al., 2016. Saikosaponin-d: a potential chemotherapeutics in castration resistant prostate cancer by suppressing cancer metastases and cancer stem cell phenotypes. Biochem Bioph Res Co 474 (4), 722–729.
Zhou, X., et al., 2014. Attenuation of neuropathic pain by saikosaponin a in a rat model of chronic constriction injury. Neurochem. Res. 39 (11), 2136–2142.
Zieminska, E., et al., 2017. The role of Ca(2+) imbalance in the induction of acute oxidative stress and cytotoxicity in cultured rat cerebellar granule cells challenged with tetrabromobisphenol A. Neurochem. Res. 42 (3), 777–787.